PNAS RESEARCH ARTICLE | PHYSICS

Generation of intense phase-stable femtosecond hard X-ray pulse pairs

Yu Zhang[a,1], Thomas Kroll[b], Clemens Weninger[c,d], Yurina Michine[e], Franklin D. Fuller[c], Diling Zhu[c], Roberto Alonso-Mori[c], Dimosthenis Sokaras[b], Alberto A. Lutman[f], Aliaksei Halavanau[g], Claudio Pellegrini[g,1], Andrei Benediktovitch[h], Makina Yabashi[i,j], Ichiro Inoue[i], Yuichi Inubushi[i,j], Taito Osaka[i], Jumpei Yamada[i], Ganguli Babu[k], Devashish Salpekar[k], Farheen N. Sayed[k], Pulickel M. Ajayan[k], Jan Kern[l], Junko Yano[l], Vittal K. Yachandra[l], Hitoki Yoneda[e], Nina Rohringer[h,m,1], and Uwe Bergmann[a,n,1]

Contributed by Claudio Pellegrini; received November 1, 2021; accepted February 2, 2022; reviewed by Ursula Keller and Markus Kowalewski

Coherent nonlinear spectroscopies and imaging in the X-ray domain provide direct insight into the coupled motions of electrons and nuclei with resolution on the electronic length scale and timescale. The experimental realization of such techniques will strongly benefit from access to intense, coherent pairs of femtosecond X-ray pulses. We have observed phase-stable X-ray pulse pairs containing more than 3×10^7 photons at 5.9 keV (2.1 Å) with ∼1 fs duration and 2 to 5 fs separation. The highly directional pulse pairs are manifested by interference fringes in the superfluorescent and seeded stimulated manganese Kα emission induced by an X-ray free-electron laser. The fringes constitute the time-frequency X-ray analog of Young's double-slit interference, allowing for frequency domain X-ray measurements with attosecond time resolution.

X-rays sciences | frequency combs | interferometry

Significance

The generation of phase-stable femtosecond X-ray pulse pairs will advance nonlinear spectroscopies and imaging, providing direct insight into the coupled motions of electrons and nuclei with resolution on the electronic length scale and timescale. This paper presents the generation of such pulse pairs in the X-ray domain. The approach uses X-ray free-electron laser pulses to induce highly directional, intense, phase-stable pairs of superfluorescence and seeded stimulated emission at the 5.9 keV manganese $K\alpha_1$ line. The finding is evidenced by strong interference fringes in the superfluorescence and stimulated emission signals.

Nonlinear coherent imaging and spectroscopy techniques have revolutionized our understanding of the structures and dynamics of molecules and materials (1–3). Mukamel and coworkers (4, 5) have proposed the extension of nonlinear optical techniques to the X-ray spectral domain to exploit the advantages of atomic spatial resolution and element sensitivity by core-level excitations. The development of powerful X-ray free-electron lasers (XFEL) has enabled new classes of experiments with unprecedented spatial resolution and femtosecond temporal resolution by various techniques (6–9), but the experimental realization of many of the proposed nonlinear X-ray techniques, such as coherent X-ray pump/X-ray probe experiments, is very challenging for lack of intense, coherent, femtosecond X-ray pulses with fixed relative phases.

The standard operation of XFELs results in self-amplified spontaneous emission (SASE) (10) pulses consisting of many random spectral and temporal spikes with limited longitudinal coherence (with coherence times for hard X-rays pulses in the subfemtosecond range). Self-seeding schemes (11) provide monochromatic XFEL pulses with increased temporal coherence, and several groups are pursuing the creation and detection of XFEL pulse pairs (12–14). However, no phase-stabilized femtosecond hard X-ray pulse pairs have been created to date. A different approach for creating intense coherent X-ray pulses is by collective spontaneous emission (15–19) and seeded stimulated emission (17, 20), which have been observed and explored in various systems at X-ray energies ranging from 850 to 8 keV. In both cases, an SASE XFEL pump pulse creates core-electron excitation of a long, quasi-one-dimensional (quasi-1D) medium in a traveling wave geometry. X-ray fluorescence photons spontaneously emitted in the entrance region along the XFEL propagation direction initiate the collective spontaneous emission along this direction (Fig. 1). In the initial stages of the process, this leads to amplified spontaneous emission (ASE), and when the collective emission becomes strong enough to overcome the decoherence rate of spontaneous emission and Auger decay, superfluorescence emerges (21, 22). The principles and applications of these inner-shell X-ray lasing phenomena are explored for spectroscopy (18, 20) and as a new X-ray source (15, 23, 24). If an XFEL SASE pump pulse contains two strong temporal spikes, these can generate two superfluorescence or seeded stimulated emission pulses that are separated by a few femtoseconds. In this report, we present experimental evidence and a theoretical description of the creation of such phase-stable X-ray pulse pairs. Evidence of these pulse pairs is provided by the observation of interference fringes in superfluorescence and seeded stimulated emission bursts of the manganese Kα fluorescence at 5.9 keV (2.1 Å).

Author contributions: T.K., C.W., Y.M., F.D.F., D.Z., R.A.-M., D.S., M.Y., I.I., Y.I., T.O., J.Y., J.K., J.Y., V.K.Y., H.Y., and U.B. performed the research; G.B., D.S., F.N.S., and P.M.A. contributed to reagents/analytical tools; Y.Z., C.W., A.A.L., A.H., C.P., A.B., N.R., and U.B. analyzed the data; and Y.Z., A.B., N.R., and U.B. wrote the paper.

Reviewers: U.K., Eidgenossische Technische Hochschule Zurich; and M.K., Stockholms Universitet.

The authors declare no competing interest.

[1]To whom correspondence may be addressed. Email: yu.spacezhang@gmail.com, claudiop@slac.stanford.edu, nina.rohringer@desy.de, or ubergmann@wisc.edu.

This article contains supporting information online at http://www.pnas.org/lookup/suppl/doi:10.1073/pnas.2119616119/-/DCSupplemental.

Published March 15, 2022.

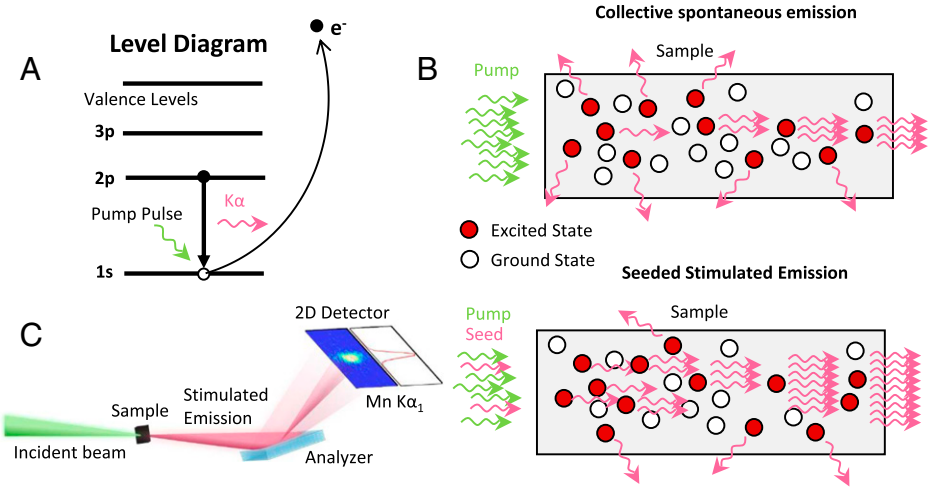

Fig. 1. The concept of inner-shell X-ray lasing and experimental setup. (*A*) Level diagram for Kα X-ray fluorescence (red) following 1s core-hole ionization by an incident photon (green). (*B*) Concepts of the two types of stimulated X-ray emission. The pump pulse (green) creates 1s core-hole excited states (red). In collective spontaneous emission (ASE and superfluorescence), a spontaneously emitted Kα photon creates amplification by stimulating the emission of a second Kα photon along the direction of 1s core-hole excited states. In seeded stimulated emission, the seed pulse photons (red) stimulate the emission of Kα photons from 1s core-hole excited states along the seeding direction. (*C*) Schematics of the experimental setup.

Results

The experiments were performed at the nanofocus instrument Experimental Hutch 5 (EH5) on beamline 3 at the (SPring-8 Angstrom Compact free electron LAser) SACLA XFEL, providing highly focused SASE pump and seed pulses (*SI Appendix* has more details on the experimental setup and pump and seed pulse parameters). Spectral analysis of the emission signal was performed using a flat Si (220) analyzer crystal dispersing the emission signal onto a two-dimensional (2D) charge-coupled device (CCD) detector with the spectral axis in the vertical direction and the spatial axis in the horizontal direction in a geometry similar to previous experiments (18, 20) (*SI Appendix*).

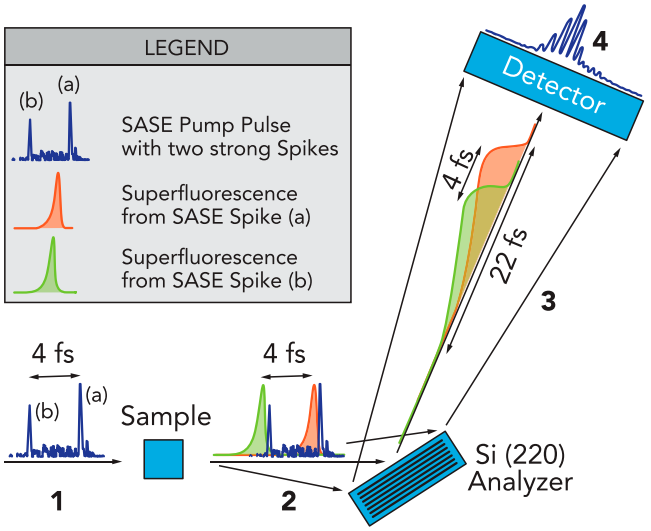

Fig. 2. Schematics of superfluorescence interference. In step 1, an SASE pump pulse with two strong spikes (a and b) separated by ~4 fs impinges on the sample, creating two subsequent superfluorescence pulses. In step 2, the transmitted SASE pulse and the two coherent superfluorescence pulses leave the sample and impinge on the analyzer. The Si (220) analyzer is set at the Bragg angle range corresponding to the Kα spectrum. It rejects the SASE pump pulse and stretches the superfluorescence pulses to ~22 fs in duration, corresponding to ~0.24 eV spectral resolution (step 3). The two stretched pulses create frequency interference along the different Bragg angles that define the dispersive axis of the detector (step 4).

In Fig. 2, we illustrate the experimental conditions for observing interference fringes. An XFEL SASE pump pulse with two strong temporal spikes (a and b) impinges on the sample (step 1), each creating a short superfluorescence burst. The two pulses leave the sample with a slight delay with respect to their respective SASE spikes given by the lifetime of the excited state (step 2). The two pulses do not overlap temporally until they impinge on the analyzer crystal, where they are spectrally dispersed and temporally stretched to ~22 fs (~8 fs full width at half maximum [FWHM]), corresponding to the ~0.24 eV FWHM Si (220) resolution (step 3). The two signals then create the frequency interference with the fringe spacings that are inversely proportional to their time delays (step 4). (*SI Appendix* has more details.)

It has been shown that at the onset of amplification, ASE and seeded stimulated emission spectra can exhibit gain narrowing (17, 18, 20). Once the superfluorescence takes over, transform limited pulses build up, and the emission spectrum features a nearly constant spectral width as the amplification increases (18) before spectral broadening and the potential buildup of damped, spectral secondary maxima sets in when approaching saturation (17–19, 23). Further increasing the pump power and/or optical density of the sample can lead to additional broadening and inhomogeneities of the spectral features as well as spatial structures. Fig. 3 *A* and *B* shows examples of broad and inhomogeneous superfluorescence emission spectra from a concentrated solid MnO sample. Also shown are spatial cuts of the spectra obtained for emission along the center direction of the pulse indicated by the white line. We observe similar signals for $MnSO_4$, Mn_2O_3, MnO_2, and Mn metal foil samples in both superfluorescence and seeded stimulated emission (*SI Appendix*). Many of the spatial emission profiles show inhomogeneities, and some show additional speckle-like features (Fig. 3B and *SI Appendix*, Fig. S2). While the origin of these features is not yet fully understood, we note that one possible explanation could be the amplification of multiple field modes starting from noise (21). A better understanding and description of the angular and spectral inhomogeneities requires a three-dimensional numerical simulation and is currently being investigated.

Strikingly, some of the spectra exhibit regularly spaced fringe patterns along the wavelength dispersive axis (spectra are in

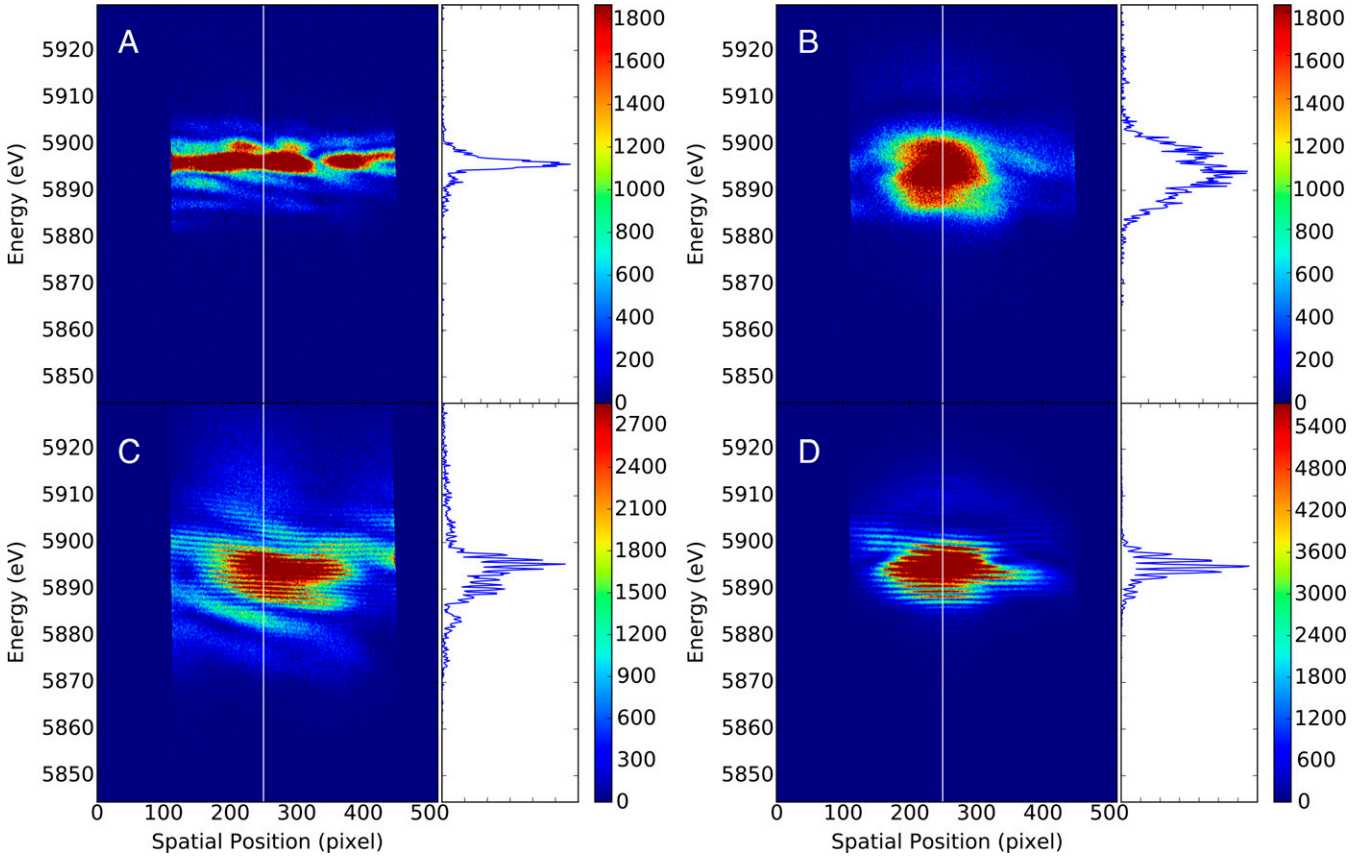

Fig. 3. Selected single-shot Kα stimulated X-ray emission spectra. In each column, the 2D spectra are shown in *Left*, where the vertical axes show the photon energy and the horizontal axes represent the spatial positions on the detector with each pixel corresponding to 50 μm size and ~15.4 μrad angular deviation from the forward direction. The 1D spectra are along the cuts (white vertical lines) at the spatial position 250 (pixel value) on the 2D spectral plane MnO (*A*–*C* without seed pulse and *D* with seed pulse) are shown in *Right*. Superfluorescence spectra with a narrow dominant peak and no obvious fringes (*A*), a broad peak and no obvious fringes (*B*), and a broad peak and fringes (*C*). Seeded stimulated emission spectrum with fringes (*D*).

Fig. 3 *C* and *D*). We observe these interference fringes in both superfluorescence and seeded stimulated emission from MnO, $MnSO_4$, Mn_2O_3, MnO_2, and Mn metal foil samples. Our analysis of several hundred single-shot fringe spectra provides the following findings (*SI Appendix* has more details): 1) occurrence of fringes is rare; 2) fringes occur in spectra with medium to high emission yields but predominantly for saturated emission; 3) fringes are generally equally spaced, with most spacings ranging from 0.8 to 1.8 eV; and 4) fringes can be present in a limited area of the spectrum or extend throughout the whole region (*SI Appendix* has a discussion of the distribution and statistics of fringe patterns). Fig. 4 *A*–*D* shows a series of fringe patterns for MnO_2 superfluorescence with spacings ranging from 0.9 to 2.5 eV and up to 3.3×10^7 estimated photons per shot after correcting for the analyzer efficiency (*SI Appendix*, Table S1).

In the following, we show with simulations how the observed fringes are related to the temporal structure of the SASE pump pulse. (*SI Appendix* has details and a discussion of how we exclude other possible causes.) Fourier analysis of the observed fringes suggests two signals separated by a time Δt related to the fringe spacings ΔE via the Planck constant $\Delta t \Delta E = h = 4.136$ fs-eV. The values for ΔE (0.9 to 2.5 eV) and corresponding values for Δt (1.7 to 4.6 fs) are shown in Fig. 4. We use the 1D semiclassical Maxwell–Bloch theory (23) to simulate the spectra (*SI Appendix* has more details). While we do not expect this simulation to reproduce the spectral profile in the saturation region, it provides emission yields for the experimental parameters and links the temporal structure of the SASE pump pulses to the observed fringes. Fig. 4 *E*–*G* shows calculated emission spectra for three different pump pulses (shown in *Insets* in Fig. 4 *E*–*G*) and evolution as a function of relative propagation distance through the gain medium. First, we approximate the SASE pump pulse by a pair of 0.5 fs FWHM Gaussian pulses with a 4 fs spacing, where the relative phase of these pulses is arbitrary (Fig. 4*E*). The simulated spectrum exhibits well-resolved fringes with ~1.0 eV spacing, showing that two spikes in the temporal profile of the pump pulse can lead to X-ray fringes in the superfluorescence. Next, we use realistic temporal profiles for the SASE pump pulses (10)—Gaussian noise—having fluctuating spectral and temporal field profiles related by the Fourier transformation (Fig. 4*F*). Corresponding spectral profiles have been measured for hard X-ray SASE pulses (25). The evolution of the emission spectrum as a function of propagation distance for such a typical SASE pump pulse and its emission spectrum at 60% relative propagation is shown in Fig. 4*E*. While there is some structure in the emitted spectrum, no clear fringe pattern arises (*SI Appendix* has detailed simulation settings of the pulse parameters). Finally, we use a realistic SASE pump pulse with two dominant temporal spikes separated by ~3.2 fs (Fig. 4*G*). In this case, interference fringes with constant spacing of ~1.25 eV arise in the superfluorescence. The fact that superfluorescence is a highly nonlinear phenomenon explains why the weaker spikes of the SASE spectrum might not lower the observed contrast of the interference fringes. A temporal spike only creates superfluorescent emission once it reaches the threshold required for sufficient population inversion. This also

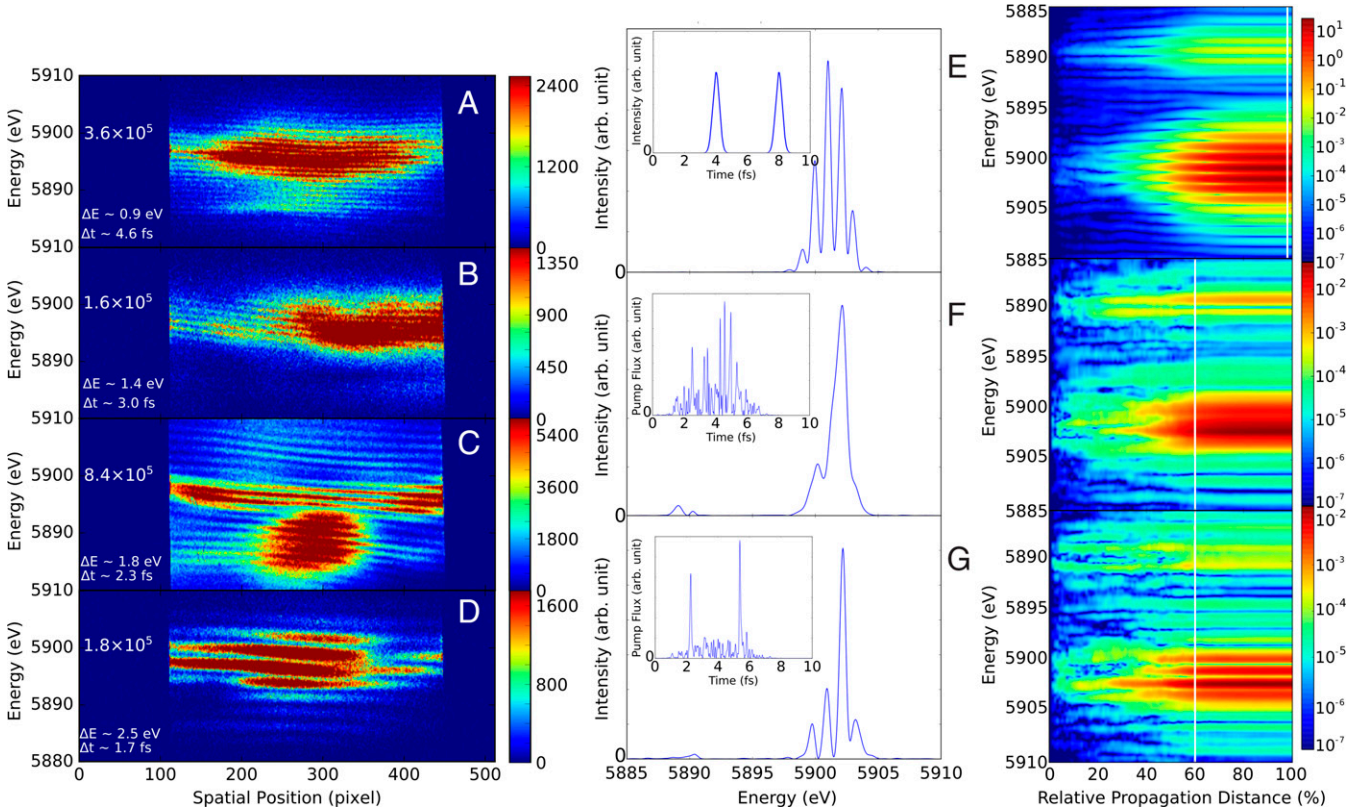

Fig. 4. Comparison of observed fringes with theory. (*A*–*D*) Selected MnO_2 superfluorescence single-shot spectra with increasing fringe spacings ΔE from ~0.9 to 2.5 eV are shown in *Left*. Corresponding time delays Δt between two pulses that cause these fringe spacings and numbers of detected photons are provided for each spectrum. Calculation of superfluorescence spectra showing interference fringes using a 1D Maxwell–Bloch model simulation with a pump pulse consisting of two equal-intensity Gaussians with 0.5 fs FWHM and 4 fs time delay (*E*), a random SASE pump pulse (*F*), and a SASE pump pulse, which has two dominant temporal spikes separated by ~3.1 fs (*G*). The depicted spectra are taken at the white cut lines in E (98%), F (60%), and G (60%) along the evolution of the calculated collective emission spectra shown as a function of relative propagation distance (percentages) of the pump pulse through the sample in *Right*.

explains why fringes are rare. Regarding the likelihood of SASE pulses with predominantly two dominant spikes separated by less than 5 fs, we note that SACLA was running in strong bunch compression mode with <8-fs pulse length. We speculate that the varying occurrence rate of fringes for different SACLA runs reflects variations in the strong electron bunch compression in the accelerator, causing different temporal profiles of the SASE pulses. Experiments and simulations using various strong bunch compression schemes at the Linac Coherent Light Source, while different from those at SACLA, have shown that strongly compressed SASE pulses can have so-called "horn-like" temporal structures that favor the likelihood of having two strong temporal spikes. We further speculate that observed fringe spectra with varying spacings are caused by modulations resulting from other spectral inhomogeneities and possibly, by SASE pulses with more than two strong spikes (*SI Appendix* has more details).

Conclusions

We have experimental evidence that X-ray superfluorescence and seeded stimulated emission generated by an XFEL SASE pulse with coherence times in the subfemtosecond range can result in phase-stable femtosecond X-ray pulse pairs. The resulting spectral fringe pattern contains the information about the temporal profile of the interfering X-ray pulses, temporal coherence, delay, and relative phase. The spectral fringe separation directly encodes the time delay of the pulses, which can be determined with subfemtosecond precision. Our simulations show that with the current experimental resolution, we should be able to measure relative fringe spacing differences of $\sim 5 \times 10^{-3}$, translating to a ~20 as precision for measuring delays of ~4 fs (*SI Appendix*). Employing an analyzer with higher-order Bragg reflection can further improve this precision and enable the discrimination of smaller fringe spacings corresponding to longer pulse delay times. The temporal intensity profile and the relative phase of the pulse pairs that remain undetermined in the current analysis can potentially be recovered by the application of reconstruction algorithms. To develop phase-sensitive nonlinear X-ray techniques, a stabilization of the relative phase of the two pulses would be required. One potential mechanism is when the temporal ringing of a superfluorescent emission seeds a second burst of superfluorescence, thereby imprinting the phase of the first pulse onto the second (*SI Appendix*). A future more robust method for obtaining phase locked pairs of femtosecond X-ray pulses by superfluorescence could be the application of seed pulses at the emission frequency that have been previously monochromatized and thus, have a temporal coherence substantially larger than the XFEL pump-pulse duration. These extensions are currently being investigated in our theoretical studies and will enable coherent nonlinear spectroscopies and nonlinear imaging in the X-ray domain (e.g., refs. 5 and 8) to study vibronic wave packets at unprecedented spatial and temporal resolution. Further improvement in the generation and control of double-superfluorescent pulse pairs will benefit from emerging XFEL pulse-shaping techniques (12, 25–31). Extending the approach beyond pulse pairs might pave the way to realizing frequency combs in the hard X-ray region.

Data Availability. All data are included in the manuscript and/or *SI Appendix*.

ACKNOWLEDGMENTS. We thank Joachim Stöhr, Robert Byer, James Cryan, Toru Hara, Shimon Kolkowitz, and Philippe Wernet for discussions and Terry Anderson for help with the figures. The experiment at SACLA was performed with the approval of the Japan Synchrotron Radiation Research Institute (proposal no. 2017B8066). Part of this work was supported by the Department of Energy (DOE), Laboratory Directed Research and Development Program at SLAC National Accelerator Laboratory under Contract DE-AC02-76SF00515 (to U.B.). Additionally, part of this work was supported by Ruth L. Kirschstein National Research Service Award F32GM116423 (to F.D.F.); Director, Office of Science, Office of Basic Energy Sciences, Division of Chemical Sciences, Geosciences, and Biosciences of the DOE Contracts DE-AC02-76F00515 (to C.P.) and DE-AC02-05CH11231 (to J.Y. and V.K.Y.); and NIH Grants GM126289 (to J.K.), GM110501 (to J.Y.), and GM055302 (to V.K.Y.). This work was supported by JPSJ KAKENHI Grant 19K20604 (to I.I.). The Stanford Synchrotron Radiation Lightsource Structural Molecular Biology Program is supported by the DOE Office of Biological and Environmental Research and NIH National Institute of General Medical Sciences (NIGMS) Grant P41GM103393. The contents of this publication are solely the responsibility of the authors and do not necessarily represent the official views of the NIGMS or the NIH.

Author affiliations: [a]Stanford PULSE Institute, SLAC National Accelerator Laboratory, Menlo Park, CA 94025; [b]Stanford Synchrotron Radiation Lightsource, SLAC National Accelerator Laboratory, Menlo Park, CA 94025; [c]Linac Coherent Light Source, SLAC National Accelerator Laboratory, Menlo Park, CA 94025; [d]MAX IV Laboratory, Lund University, Lund 224 84, Sweden; [e]Institute for Laser Science, The University of Electro-Communications, Chofu,Tokyo 182-8585, Japan; [f]Linac & FEL Division, SLAC National Accelerator Laboratory, Menlo Park, CA 94025; [g]Accelerator Research Division, SLAC National Accelerator Laboratory, Menlo Park, CA 94025; [h]Center for Free-Electron Laser Science CFEL, Deutsches Elektronen-Synchrotron DESY, Hamburg 22607, Germany; [i]RIKEN SPring-8 Center, Sayo-cho, Sayo-gun, Hyogo 679-5148, Japan; [j]Japan Synchrotron Radiation Research Institute, Sayo-cho, Sayo-gun, Hyogo 679-5198, Japan; [k]Department of Materials Science and NanoEngineering, Rice University, Houston, TX 77005; [l]Molecular Biophysics and Integrated Bioimaging Division, Lawrence Berkeley National Laboratory, Berkeley, CA 94720; [m]Department of Physics, Universität Hamburg, Hamburg 20355, Germany; and [n]Department of Physics, University of Wisconsin–Madison, Madison, WI 53706

1. W. Min, C. W. Freudiger, S. Lu, X. S. Xie, Coherent nonlinear optical imaging: Beyond fluorescence microscopy. *Annu. Rev. Phys. Chem.* **62**, 507–530 (2011).
2. E. Collini, 2D electronic spectroscopic techniques for quantum technology applications. *J. Phys. Chem. C Nanomater Interfaces* **125**, 13096–13108 (2021).
3. A. Ghosh, J. S. Ostrander, M. T. Zanni, Watching proteins wiggle: Mapping structures with two-dimensional infrared spectroscopy. *Chem. Rev.* **117**, 10726–10759 (2017).
4. S. Mukamel, D. Healion, Y. Zhang, J. D. Biggs, Multidimensional attosecond resonant X-ray spectroscopy of molecules: Lessons from the optical regime. *Annu. Rev. Phys. Chem.* **64**, 101–127 (2013).
5. M. Kowalewski, B. P. Fingerhut, K. E. Dorfman, K. Bennett, S. Mukamel, Simulating coherent multidimensional spectroscopy of nonadiabatic molecular processes: From the infrared to the X-ray regime. *Chem. Rev.* **117**, 12165–12226 (2017).
6. C. Bostedt *et al.*, Linac coherent light source: The first five years. *Rev. Mod. Phys.* **88**, 015007 (2016).
7. U. Bergmann *et al.*, Using X-ray free-electron lasers for spectroscopy of molecular catalysts and metalloenzymes. *Nat. Rev. Phys.* **3**, 264–282 (2021).
8. J. P. Marangos, Accessing the quantum spatial and temporal scales with XFELs. *Nat. Rev. Phys.* **2**, 332–334 (2020).
9. K. Asakura, K. J. Gaffney, C. Milne, M. Yabashi, XFELs: Cutting edge X-ray light for chemical and material sciences. *Phys. Chem. Chem. Phys.* **22**, 2612–2614 (2020).
10. R. Bonifacio, L. De Salvo, P. Pierini, N. Piovella, C. Pellegrini, Spectrum, temporal structure, and fluctuations in a high-gain free-electron laser starting from noise. *Phys. Rev. Lett.* **73**, 70–73 (1994).
11. J. Amann *et al.*, Demonstration of self-seeding in a hard-X-ray free-electron laser. *Nat. Photonics* **6**, 693–698 (2012).
12. N. Hartmann *et al.*, Attosecond time-energy structure of X-ray free-electron laser pulses. *Nat. Photonics* **12**, 215–220 (2018).
13. J. Duris *et al.*, Tunable isolated attosecond X-ray pulses with gigawatt peak power from a free-electron laser. *Nat. Photonics* **14**, 30–36 (2020).
14. D. Gauthier *et al.*, Chirped pulse amplification in an extreme-ultraviolet free-electron laser. *Nat. Commun.* **7**, 13688 (2016).
15. N. Rohringer *et al.*, Atomic inner-shell X-ray laser at 1.46 nanometres pumped by an X-ray free-electron laser. *Nature* **481**, 488–491 (2012).
16. C. Weninger *et al.*, Stimulated electronic x-ray Raman scattering. *Phys. Rev. Lett.* **111**, 233902 (2013).
17. H. Yoneda *et al.*, Atomic inner-shell laser at 1.5-ångström wavelength pumped by an X-ray free-electron laser. *Nature* **524**, 446–449 (2015).
18. T. Kroll *et al.*, Stimulated x-ray emission spectroscopy in transition metal complexes. *Phys. Rev. Lett.* **120**, 133203 (2018).
19. L. Mercadier *et al.*, Evidence of extreme ultraviolet superfluorescence in xenon. *Phys. Rev. Lett.* **123**, 023201 (2019).
20. T. Kroll *et al.*, Observation of seeded Mn Kβ stimulated X-ray emission using two-color x-ray free electron laser pulses. *Phys. Rev. Lett.* **125**, 037404 (2020).
21. M. Gross, S. Haroche, Superradiance: An essay on the theory of collective spontaneous emission. *Phys. Rep.* **93**, 301–396 (1982).
22. A. Benediktovitch, V. P. Majety, N. Rohringer, Quantum theory of superfluorescence based on two-point correlation functions. *Phys. Rev. A (Coll. Park)* **99**, 013839 (2019).
23. C. Weninger, N. Rohringer, Transient-gain photoionization x-ray laser. *Phys. Rev. A* **90**, 063828 (2014).
24. A. Halavanau *et al.*, Population inversion X-ray laser oscillator. *Proc. Natl. Acad. Sci. U.S.A.* **117**, 15511–15516 (2020).
25. D. Zhu *et al.*, A single-shot transmissive spectrometer for hard X-ray free electron lasers. *Appl. Phys. Lett.* **101**, 034103 (2012).
26. Y. Inubushi *et al.*, Determination of the pulse duration of an x-ray free electron laser using highly resolved single-shot spectra. *Phys. Rev. Lett.* **109**, 144801 (2012).
27. T. Hara *et al.*, Two-colour hard X-ray free-electron laser with wide tunability. *Nat. Commun.* **4**, 2919 (2013).
28. S. Huang *et al.*, Generating single-spike hard X-ray pulses with nonlinear bunch compression in free-electron lasers. *Phys. Rev. Lett.* **119**, 154801 (2017).
29. A. Marinelli *et al.*, Experimental demonstration of a single-spike hard-X-ray free-electron laser starting from noise. *Appl. Phys. Lett.* **111**, 151101 (2017).
30. S. Li *et al.*, Characterizing isolated attosecond pulses with angular streaking. *Opt. Express* **26**, 4531–4547 (2018).
31. S. Reiche *et al.*, A perfect X-ray beam splitter and its applications to time-domain interferometry and quantum optics exploiting free-electron lasers. *Proc. Natl. Acad. Sci. U.S.A.* **119**, e2117906119 (2022).